Energy and phase relaxation accompanying impulsive reactions in liquids



1996 J. Phys.: Condens. Matter 8 9201

(http://iopscience.iop.org/0953-8984/8/47/009)

J. Phys.: Condens. Matter **8** (1996) 9201–9220. Printed in the UK

# Energy and phase relaxation accompanying impulsive reactions in liquids

S Gnanakaran, M Lim, N Pugliano†, M Volk‡ and R M Hochstrasser

Department of Chemistry, University of Pennsylvania, Philadelphia, PA 19104-6323, USA

Received 3 October 1996

**Abstract.** Experiments made possible by new laser methods explore ultrafast features of solution phase reaction dynamics. The results from two examples are given. Photodissociation of small molecules such as $HgI_2$ and $OCl^-$ in solution yields highly excited vibrational state distributions and narrow bond length distributions. The dynamics in the transition state region and the ensuing dynamics can be followed by femtosecond laser experiments that probe the phase and energy loss processes.

The mercuric iodide experiments show that the phase relaxation is dominated by coherence transfer processes which have a strong analogy to classical motions. The population relaxation dynamics gives results similar to those from classical molecular dynamics simulations which suggest, notwithstanding the significant polarity of the molecules and solvents, that the relaxations are dominated by Lennard–Jones repulsion at sufficiently low frequencies.

## 1. Introduction

This paper is concerned with the ultrafast features of reaction dynamics in solutions where much of conventional chemistry occurs. Obviously the observables associated with solution phase reactions are different from those that are traditional for gas phase processes. In the latter, scattering experiments yield information regarding the distribution of eigenstates of the reaction products corresponding to those of reactants. The nature of the reactive processes can be deduced from this information [1]. More recently, femtosecond pump/probe laser experiments on isolated molecules have confirmed many of the ideas from these scattering experiments and further exposed the transition state dynamics of molecules [2]. In the condensed phase, the time domain methods were always necessary in studies on reaction dynamics because the interactions with the solvent not only help create, but also destroy the information about the product states that are generated in the reaction [3]. Even simple scattering type experiments when carried out in solutions require ultra-short time resolution if information on the energy distributions is to be obtained. The understanding of reaction dynamics in solutions has been greatly advanced by theoretical studies [4–10] and recent experimental work [11–24] on small molecules. The experiments generally involve ultrafast laser studies of photodissociation, photoisomerization, geminate (or cage) reactions and the vibrational relaxation of molecules. We describe herein experiments on

† Present address: Rohm and Haas Company, Research Laboratories, 727 Norristown Road, Box 904, Spring House, PA 19477-0904, USA.

‡ Present address: Institut für Physikalische und Theoretische Chemie, TU München, Lichtenberg Straße. 4, 85748 Garching, Germany.

0953-8984/96/479201+20$19.50  

two photoreactions, the results of which are complemented by classical molecular dynamics simulations.

The first reaction involves the photodissociation of $HgI_2$ in ethanol [22–25] to the polar HgI fragment. The analogous gas phase reaction produces HgI molecules that are in highly nonequilibrium coherent states [26–28]. Unlike the situation for the gas phase reaction, the presence of solvent gives rise to energy transfer to and from the solvent modes. The solvent also can have a role in the energy release mechanisms near the transition state and as the reaction products proceed toward thermal equilibrium. This system can be used as a prototype to study the wavepacket motion [22, 25], vibrational relaxation [23, 29], and properties of the transition state in solvents [30].

The second reaction concerns a system having very strong solute–solvent coupling. The water solvated $ClO^-$ ion which undergoes rapid inter-atomic electron transfer (charge shifting) upon light absorption [31, 32]. *Ab initio* calculations show that in the ground state the negative charge of $ClO^-$ is located on the O atom [31, 33]. Upon excitation to a Frank–Condon (FC) excited electronic state, the negative charge can shift to the Cl atom generating a nonequilibrium solvent configuration. After charge shifting it is expected that the solvent structure around the O atom will rapidly decay and that around $Cl^-$ will form. The possibility of optically induced charge shifting from $O^-$ to Cl is examined as is the back electron transfer process, $OCl^- \rightarrow ClO^-$ [32]. It represents a particularly interesting reaction to study in a solution of polar molecules because the charge shifting event that accompanies this reaction obviously couples to the polar solvent molecules degrees of freedom [9]. Such a situation permits an opportunity to evaluate whether the solvent adiabatically couples to the reactive motion or if its response is too slow, thus generating a highly nonequilibrated transient solvent state. Thus, this system will be used as a proto-type to study the solvent response to a charge shifting [32].

To gain proper understanding of the reactions of even small molecules in solutions, a wide range of structural and dynamical effects need to be characterized. The knowledge of the relaxation parameters and reorientational dynamics and the effect of solvent friction on them is needed to understand the relaxation of the vibrational coherence and populations of vibrational states. Although it is instructive to compare condensed phase experiments and those of isolated molecules, it is clear that the way in which solvated reactions are to be discussed must involve a statistical approach [3]. An important equilibrium solvent effect on chemical reactions is the alteration of the free energy surfaces and barriers because reactants and products at various internuclear separations may be solvated more or less effectively than the transition state intermediates. Dynamic aspects of the solvent effect, which can change the rate and outcome of a reaction critically, depend on how the solvent responds to changes in the charge distributions of reactants. In the case of a reaction involving polar molecules in a polar solvent, the coupling to the solvent depends on the relative rates of the intrinsic reaction and the solvent response to charge redistribution of the reacting species [34]. We are not concerned here with the case of high, narrow barrier reactions for which the solvent may play very little role other than as a means for energizing the reactants [10].

The influence of the nonequilibrated solvent can also be examined under conditions in which the period of reactive motion and the vibrational periods of the parent and products are similar to, or faster than, the decay of the solvent correlation function. For the situation in which the solute vibrational motions occur on comparable timescales with those of coupled solvent modes, a multidimensional reaction coordinate that incorporates the solvent must be considered. Other systems might be in a limit in which the solvent can easily follow the solute motions or even that the solvent simply senses a vibrationally averaged structure. These are just extreme situations and a full treatment needs to connect the nonadiabatic

limit to that of an equilibrium solvent coordinate [3]. We will see that the manner in which energy is partitioned and by which the synchrony of nuclear motions in the reactant state (coherence) is transferred into the products of a reaction will depend on these conditions. Further efforts along these lines will bring the study of solvated chemical reactions to the level of requiring accurate calculations of the solute–solvent intermolecular forces. These forces are typically treated in terms of average properties. However, impulsive reactions may produce specific cooperative states of the solvent shell. Experiments are needed to determine accurate, solvated potential energy surfaces of small molecules in solution.

The information acquired by time resolved spectroscopy regarding the dynamics of chemical reactions in solution can be significantly extended by carrying out the experiments in polarized light. Such experiments yield the pump/probe anisotropy which is proportional to the difference between the signal obtained with pump and probe pulses polarized parallel and perpendicular to one another. It permits the determination of the symmetry characteristics of transitions which in turn helps to establish the nature of the electronic states involved in the reaction. It also can enable the detection of coherence and the measurement of coherence loss [35]. The rotations of the transition dipoles, the reactant, the transition states and the products of the reaction can also be determined [36]. In addition, the anisotropy can help unravel the complex kinetic behaviour that can arise from overlapping signals of different species that are rotating and are involved in a reaction [37, 38]. Different solvent configurations may lead to different solute structures and hence to inhomogeneties in the ensemble of reactive trajectories. This spreads the distribution of equilibrium geometries in the solution, and therefore changes the concept of the transition state to an average, solvent mediated property [3]. We will choose the example of the photodissociation of $HgI_2$ in ethanol to picture transition state dynamics in a solution phase reaction [30]. The anisotropy can be used to examine the angular motion as the nuclei move through the transition state and the rotational energy distribution.

Studies of diatomic solutes are particularly valuable because the influence of external solvent forces acting on the single mode without interference from other *internal* modes can be studied. The inherent phase coherence throughout the ensemble of products is altered by the coupling to the bath of solvent states [25]. Solvent induced modifications of the potential energy surfaces may also be influential in altering reactive trajectories, as well as the product state partitioning of energy. All of these solvent frictional effects can be addressed by monitoring the details of both the population and coherence relaxation associated with the vibrational and electronic levels involved. If the time resolution used in experiments is shorter than the vibrational period then the energy eigenstates are not seen separately. With these conditions it is more convenient to discuss the dynamics in terms of eigenstates of the displacement of the nuclei from their equilibrium positions. Each of these is, of course, a superposition of energy eigenstates. The ensemble of molecules thus prepared has a coherent polarizability, oscillating in response to the in-phase vibrational motion of all the molecules: clearly the reactions generate products that are described by a wavepacket, constituted by a definite set of energy states and their associated phases.

All the observables of systems undergoing motion and relaxation in bound states can be determined in principle from the density matrix of the wavepacket. A key property is the probability density that a product molecule will have displacement $x$, at time $t$, which when given in terms of the density matrix $\rho$, as:

$$P(x,t) = \langle x|\,\rho(t)\,|x\rangle = \sum \phi_m^*(x)\phi_n(x)\rho_{mn}(t) \tag{1}$$

permits the propagation of the wavepacket $P(x,t)$ based on the energy eigenstates ($\phi_n(x)$) if these are known. The dynamics of the density matrix, while known exactly in the gas

phase for a known surface [39], in general needs information about the coupling of the diatomic molecule to the solvent. When the eigenfunctions are not at all known, one can still propagate the wavepacket by direct numerical solution of the Schrodinger equation [40] on an approximate potential surface. Second-order relaxation theory [41], an example of which is Redfield theory [42], can be used to calculate the reduced density matrix elements needed in equation (1), through the relaxation equations:

$$\dot{\rho}_{mn}(t) = -\mathrm{i}\omega_{mn}\rho_{mn}(t) + \sum_{pq}\Gamma_{mnpq}\rho_{pq}(t). \tag{2}$$

The relaxation parameters $\Gamma_{mnpq}$ are directly related to correlation functions of the solvent bath. When $m = n$ and $p = q = m$ they are the population state-to-state rate constants that determine the $T_1$ relaxation of the oscillator. When $m \neq n$ and $p \neq q$ they represent the coherence loss ($m = p,\ n = q$), corresponding to the $T_2$ relaxation of each pair of levels and coherence transfer ($m \neq p,\ n \neq q$), corresponding to the medium induced transfer of coherence from one level pair to another.

Much of the essential physics of coherence and population relaxation can be learned from the results of a harmonic oscillator linearly coupled to a harmonic bath. In the case that there is energy relaxation characterized by a time $T_1$ and quadratic pure dephasing, $T_2'$,

$$1/T_1 = \frac{2\pi}{\hbar}\sum_i |u_i|^2\delta(\hbar\omega_0 - \hbar\omega_i) \tag{3a}$$

$$1/T_2' = \frac{8\pi}{\hbar}\bar{n}\sum_i |u_i|^2\,\delta(\hbar\omega_i) \tag{3b}$$

where $u_i$ is the coupling of the system to the $i$th bath oscillator, $\omega_0$ is the oscillator frequency including any shift due to coupling to the bath and $\bar{n}$ is the Boson occupation number at the oscillator frequency. The master equations for the evolution of the populations and coherence involving all the Bohr frequencies are given by [41].

$$\dot{\rho}_{nn} = -\frac{1}{T_1}\left\{[n + (2n+1)\bar{n}]\rho_{nn} - (\bar{n}+1)(n+1)\rho_{n+1,n+1} - n\bar{n}\rho_{n-1,n-1}\right\} \tag{4}$$

$$\dot{\rho}_{m,m+n} = \mathrm{i}\omega_0 n\rho_{m,m+n} - \frac{1}{T_1}\left[\left\{(\bar{n}+\tfrac{1}{2})(2m+n) + \bar{n}\right\}\rho_{m,m+n} - \bar{n}\sqrt{m(m+n)}\rho_{m-1,m+n-1}\right.$$
$$\left. -(\bar{n}+1)\sqrt{(m+1)(n+m+1)}\;\rho_{m+1,m+n+1}\right] - \frac{n^2}{T_2'} \tag{5}$$

where $\hat{n}$ $(= b^\dagger b)$ is the number operator for the oscillator. From these equations it is straightforward to find and solve the equations of motion for the average energy $\langle E\rangle(t)$ and the average coordinate of the oscillator $\langle x\rangle(t)$. The results are exact and resemble those found from classical mechanics:

$$\langle E\rangle(t) = \langle E\rangle(\infty) + \mathrm{e}^{-t/T_1}\left(\langle E\rangle(0) - \langle E\rangle(\infty)\right) \tag{6}$$

$$\langle x\rangle(t) = \langle x\rangle(0)\,\mathrm{e}^{-t/T_2}\left\{\cosh\Omega t + \frac{1}{2T_1\Omega}\sinh\Omega t\right\} \tag{7}$$

where

$$\frac{1}{T_2} = \frac{1}{2T_1} + \frac{1}{T_2'} \text{ and } \Omega^2 = (1/2T_1)^2 - \omega_0^2.$$

These results tell us that we need not be concerned with the state-to-state dynamics in considering the energy relaxation or the motion of the wavepackets on a harmonic surface. Presumably this is also appropriate for surfaces that are not too anharmonic. Equation (7)

is the same result that pertains for a classical Brownian particle in a harmonic force field [43] where $T_2$ is identified with the dynamical friction [44].

The relaxation is often treated by linear response theory [45], according to which the approach to equilibrium of the perturbed system is determined by the random microscopic fluctuations of the equilibrated system. More precisely, the decay of the equilibrium time correlation function of the microscopic fluctuations should coincide with the relaxation of the macroscopic system. These time correlation functions [46] are calculated from equilibrium molecular dynamics (MD) simulations. Such simulations have become valuable in understanding many kinds of chemical reactions in solution [47–49].

As mentioned above, the vibrational energy dissipation can be thought of as the effect of solvent friction on the vibrational coordinate. In which case, one needs to understand the role of frequency dependent friction on the relaxation dynamics and the type of interactions, short-ranged or long-ranged, that dominate the friction. The fast relaxation of population is critical to the description of the dephasing dynamics, as well as being important for understanding activated processes in the condensed phase. For these reasons classical molecular dynamics simulations were employed to calculate the vibrational relaxation of HgI and $ClO^-$, and to determine the nature of the solvent forces involved. Furthermore, the simulations were used to study the isotope effect on vibrational relaxation of $ClO^-$. The simulations yielded the classical force–force autocorrelation function. This function is defined by the high temperature version of the friction spectrum through the familiar Landau–Teller expression for $T_1$ as [10, 21, 29, 50–57]

$$\frac{1}{T_1} = \frac{\zeta_{cl}(\omega)}{\mu} \tag{8}$$

in which $T_1$ is the fundamental relaxation time, $\mu$ is the reduced mass and $\zeta_{cl}(\omega)$ is the frequency dependent friction. The friction spectrum is the Fourier transform of the force autocorrelation function which is calculated from equilibrium MD simulations. This approach was used previously to calculate $T_1$ for $CH_3Cl$ treated as a diatomic [10, 50], $I_2$ [58], $I_2^-$ [58], and $N_3$ [59].

Equilibrium molecular dynamics simulations can help to generate a microscopic interpretation of the experimental measurements of the rotational dynamics as well. Both the relevant orientational correlation function, $\langle P_2(\cos\theta)\rangle$, where $\theta$ is the angle between the pumped and probed dipoles, and the rotational energy correlation function, $\langle \delta E(0)\delta E(t)\rangle$, can be calculated by standard methods from classical trajectories [46, 60], and have been reported for a number of diatomic molecules [61–66]. Interesting theoretical questions remain concerning the relationship between these two quantities. As yet there are no direct measurements of rotational energy relaxation in liquids to the best of our knowledge. In the present work we combine equilibrium simulations of the reactive, inertial-like and diffusive rotational dynamics with the results of measurements of photodissociation reactions.

## 2. Experimental examples

### *2.1. Mercuric iodide dissociation*

In the experiments the $HgI_2$ is excited by femtosecond pulses into a region where the bonds are compressed relative to HgI along the totally symmetric mode and vertically excited along the asymmetric stretch coordinate. Motion on the excited state surface begins with trajectories that are combinations of these stretches. The bending motions have a period of about 2 ps and are too slow to displace much during the reactive motion. At the beginning

of the motion the situation is probably similar to that in the gas phase [26–28] but the relaxation processes can cause energy exchange with the medium on a timescale faster than the vibrational periods. Furthermore the IHgI molecule cannot be precisely linear because of dynamic solvent structuring. There is a large anisotropic force on the separating fragments (I and HgI) which generates the distribution of internuclear separations of HgI characterizing the initially observed wavepacket. In the experiment [22–24], the reactive region and the HgI are probed by measuring the transient absorption at various optical frequencies. The first peak in the signal appears when the HgI first reaches the attractive portion of its potential surface. This takes a time of 0.45 of one HgI stretching period (i.e. 120 fs), which is determined by the repulsive forces on the reactive potential. As the wavepacket proceeds along the exit channel the attractive side of the ground state of HgI is probed on each successive cycle.

*2.1.1. Vibrational dynamics: macroscopic picture.* As mentioned above, each molecule of HgI is produced as a superposition of vibrational eigenstates on its $X$-potential function [22]. As a result there is an observable ensemble coherence or oscillating macroscopic polarizability that is related to the vibrational dynamics of the diatomic product fragments. The polarizability is detected through time resolved electronic absorption spectroscopy as a periodic variation of the transmitted probe field induced macroscopic polarization. The HgI superposition state is composed of a wide distribution of vibrational eigenstates which all posses a distinct phase relationship with respect to one another. If the probe laser is chosen to mainly interrogate a small fraction of eigenstates within the wavepacket, the oscillatory portion of the transient signal is representative of the dynamics of those vibrational levels. This is illustrated in figure 1 by the three vertical transitions that give rise to the transient absorption signals at the specified probe wavelengths. This provides an opportunity to examine vibrational level dependent solvent induced relaxation dynamics. According to the conventional models for dephasing, the relaxation rates responsible for phase dissipation in the ensemble should increase with the HgI vibrational quantum number. This was experimentally indicated by examining the dephasing rate dependence on the probe wavelength which verified that probed level pairs lying high in the HgI anharmonic potential dephase much faster than those low in the well.

*2.1.2. Population decay.* After the phase coherence in the system is completely lost, the ensemble of HgI molecules remains in a vibrationally hot distribution that can be characterized by its diagonal density matrix at each time. The evolution of this nonequilibrated population distribution gives rise to signal variations that show a wavelength dependence indicative of the population shifting amongst the HgI vibrational levels as the molecule loses energy and approaches thermal equilibrium. The signature of this relaxation is found in the longer time portion of the transient absorption signals [23]. Different portions of the vibrationally hot distribution of product molecules, generated through the dissociation reaction, are interrogated with different probe frequencies. As for the coherent portions of the signals, low energy probes sample high energy portions of the HgI population distribution, whereas high energy probes provide information on the low energy vibrational states of the well. The expected fast population relaxation for levels high in the well are evidenced by the long wavelength probe signals that exhibit an early time transient absorption that rapidly decays [23]. This energy relaxation from high lying levels feeds the lower levels on a picosecond timescale and this is detected with short wavelength probes as a rising signal that peaks, and then subsequently decays slowly to an equilibrated signal

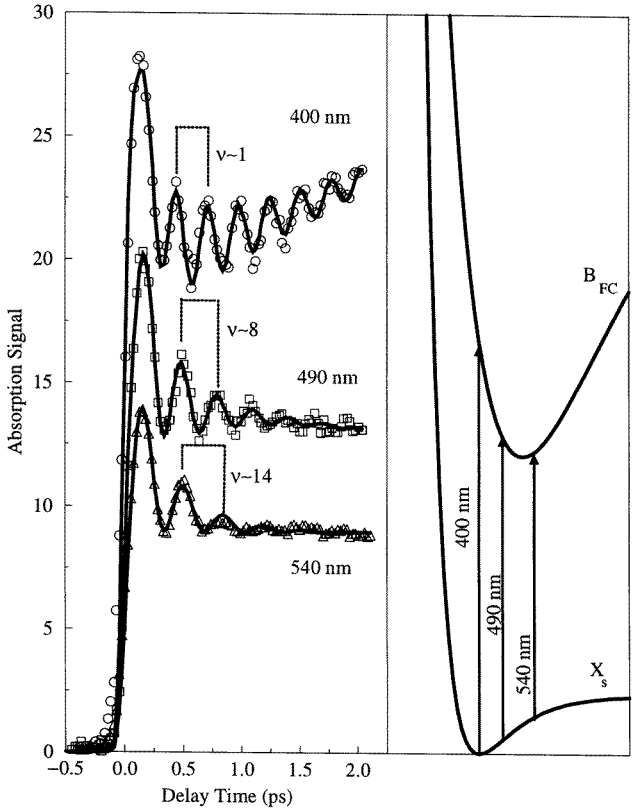


**Figure 1.** Representative transient absorption signals are shown for three probe centre wavelengths of 400 nm, 490 nm and 540 nm that probe different regions of the ground state ($X_s$) of HgI.

level.

These dynamics could be modelled with a population master equation that incorporated the anharmonicity of the HgI solute and a density of solvent states described by the power spectrum of neat ethanol [23]. The master equation was based on the assumption that the solute vibrational energy is transferred into the solvent vibrational modes. Simulated molecular responses are overlaid atop the data shown in figure 2 for the $n'' = 1 \rightarrow 0$ relaxation times of 2, 3 and 4 ps. All of the wavelength dependent data were reproduced best with the 3 ps value. It decays nonexponentially but the deviations from exponential do not exceed $\sim$ 10%. On the other hand, the master equation used to interpret the data contained anharmonically induced processes that were not negligible [23]. The simulations of the data also provided an estimate of about 1200 $cm^{-1}$ for the initial excess energy of the HgI produced by the photodissociation.

*2.1.3. Coherence decay.* After a wavepacket is launched, it begins to oscillate at the $N(N-1)/2$ Bohr frequencies of the eigenstate distribution of an anharmonic well with $N$ levels weighted according to their contribution to the superposition state. All of these natural frequencies for the isolated molecule are represented in the waveform probed by the femtosecond pulse. The dephasing of the wavepacket propagating on the HgI surface is

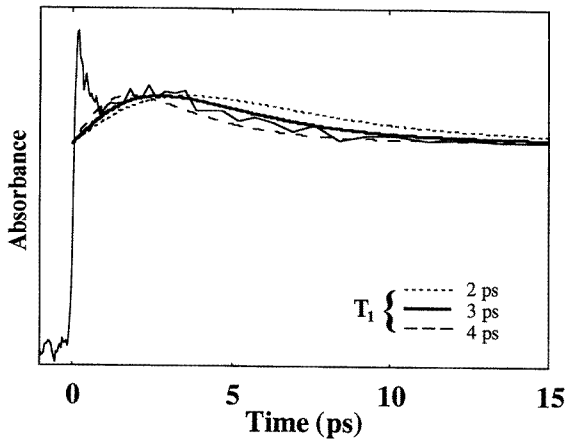


**Figure 2.** A longer time transient is shown to illustrate the signal component that grows to a maximum, and then subsequently decays indicating that the bottom of the well is being probed.

partially influenced by the phase mismatches from the different Bohr frequencies for the level pairs contributing to $|\Psi(t)\rangle$. This spreading of the wave packet represents a coherence loss process. In solution phase there also exists additional, presumably irreversible, dephasing. The models for coherence loss naturally incorporate all of these processes.

The experimentally measured population dynamics provides a value of 3 ps for the $n'' = 1 \rightarrow 0$ relaxation time. If the oscillator were harmonic this would be the $T_1$ relaxation time for the system and this would determine the amount of energy in the HgI oscillator at each instant. According to the conventional models for dephasing of two level systems, the relaxation rates responsible for phase dissipation in the ensemble should increase with the HgI vibrational quantum number. For example, if a harmonic solute that is linearly coupled to a bath of harmonic oscillators is considered, the state-to-state population decay rate is proportional to the quantum number, as indicated in equation (5), so at $n = 15$ a relaxation time out of that level is expected to be $\sim$ 200 fs. Combining this relaxation process with a pure dephasing effect, the coherence decay timescales would be predicted to lie in the sub-100 fs range for level pairs 1/3 of the way up the HgI potential. As was seen in the development of equation (7) this is not the correct way to think about relaxation in a multilevel system. The coherence transfer terms have a significant effect and can be seen from the following simple argument. Consider the coherence in the level pair $(n,\ n-1)$. The population relaxation from $n \rightarrow n-1$ and from $n+1 \rightarrow n$ occur with approximately the same rate constants if $n \gg 1$. If $\omega_{n+1,n} \approx \omega_{n,n-1}$, relaxation from levels $n$ and $n+1$ to levels $n-1$ and $n$ will not significantly alter the ensemble coherence oscillating at the frequency $\omega_{n+1,n}$. If the pure dephasing is slow compared with this relaxation there will be no loss of coherence during this population exchange process. In the case of HgI, the population decay times are ultrafast for high quantum numbers [23] and these may exceed the pure dephasing times arising from the adiabatic energy fluctuations. In this limit it is straightforward to use known principles [41] and implement equation (1) together with equation (5) to obtain the ensemble coherence. A consideration of the terms in equation (2) that transfer coherence indicates that when population relaxation rates are large and the frequency of the vibration is low enough compared with $k_B T$ (to allow significant probability for upward transitions to occur), then the coherence will be maintained. Our data appear

to be in accord with the simple theoretical prediction of equations (5) and (7) [25]. The equivalence of equation (7) with the Brownian harmonic oscillator suggests also that the Brownian oscillator Green function could be used to propagate the wavepacket. In fact the quantum Green function is essentially of the same form [43] and it is possible to fit the HgI wavepacket dynamics with Chandrasekhar's classical Green function [43]. The coherence transfer terms, for example $\Gamma_{mnm'n'}$ with $mn$ and $m'n'$ representing different level pairs are the key factors that lead to the relaxation dynamics of the quantum oscillator acquiring the classical behaviour described by equations (6) and (7).

*2.1.4. Classical picture of wavepacket dynamics.* As demonstrated above when the population relaxation is very fast, which is the case as in most of the examples given, the wavepacket dynamics is also controlled by $T_1$ relaxation [25]. When $T_1$ is much smaller than the vibrational period it is easy to see that state-to-state relaxation will not destroy the coherence since the energy changes without there being much disturbance of the distribution of nuclear coordinates. This is a situation where a simple classical model is useful because information about the eigenstates themselves is not helpful in visualizing the evolution of the spatial location and shape of a wavepacket. The system behaves much like a classical ball rolling on an anharmonic surface with friction. Within this picture, the classical analogy between wavepacket motion illustrated in figure 3(A) and classical particle-like behaviour can be made. For example in the strongly overdamped limit a distribution on the potential surface moves toward its equilibrated resting position without any possibility for the existence of recurrences. If energy relaxation in the system is fast compared with the coherence loss time and the oscillation period, the packet can essentially slide down one side of the potential while remaining a narrow distribution in $r$. This is illustrated in figure 3(B) and is considered to be important for the high energy level pairs ($< n = 15$) in the HgI system. If the packet loses energy on a timescale that is slower than the oscillation period, the wavepacket would exhibit recurrences during the relaxation. This situation corresponds to a moderately damped particle oscillating on its harmonic surface, and is illustrated in figure 3(C). In the eigenstate basis both of these cases correspond to coherence transfer under different relaxation conditions.

Even pure dephasing can be thought of from a classical point of view. The nature of adiabatic dephasing originates in the stochastic energy fluctuations imparted by the bath on the potential energy function of the system. The effect of these random energy fluctuations is to delocalize the distribution of position eigenstates, as illustrated in figure 3(D). All of these features are readily illustrated by propagating the wavepacket of choice with the classical propagator function [43] for a harmonically bound particle undergoing Brownian motion.

*2.1.5. Vibrational dynamics: microscopic picture.* The transfer of vibrational energy from the solute directly into motions of the solvent is an important form of friction that influences the motion along reaction coordinates. MD simulations have been used to calculate the friction on HgI vibrational coordinates due to ethanol solvent [29]. The calculated friction spectrum is shown in figure 4. As mentioned in the introduction, $T_1^{-1}$ is just the amplitude of the friction spectrum at the HgI oscillator frequency. At the gas phase frequency of HgI (125 $cm^{-1}$), the calculated $T_1$ time is $\sim$ 2 ps. This is in good agreement with the experimentally determined $T_1$ time of $\sim$ 3 ps. In order to understand how the coulombic forces influence the vibrational relaxation, a set of simulations were run with no partial charges on HgI. The corresponding friction spectrum is also shown in figure 4. The $T_1$

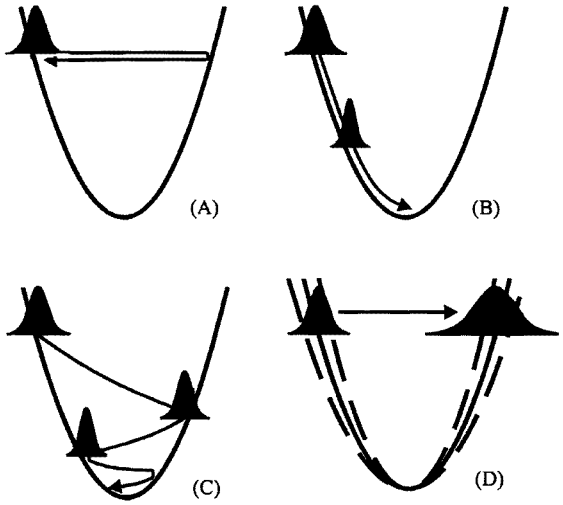


**Figure 3.** Wave packet dynamics are illustrated through classical simulations. (A) Free motion, (B) coherence transfer in the overdamped limit, (C) coherence transfer in the underdamped limit, (D) pure dephasing.

time of $\sim 3$ ps in this case is slightly longer than that obtained with charges. This result indicates that the relaxation rate does not strongly depend on coulombic interactions.

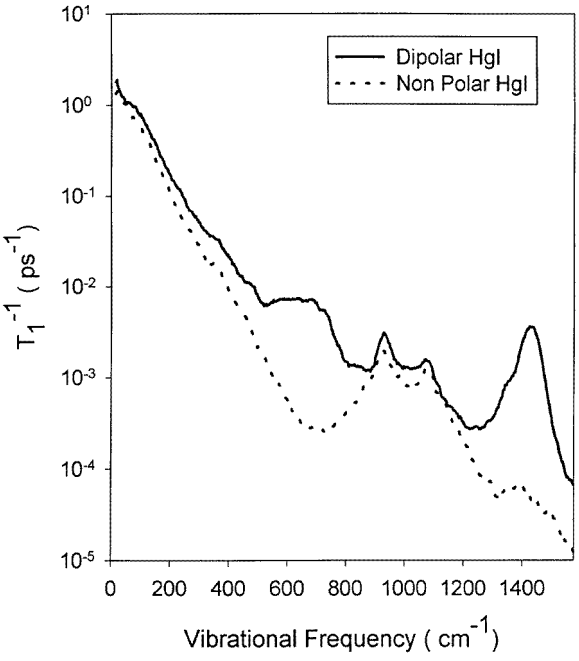


**Figure 4.** The frequency dependent friction from classical simulations for polar (solid line) and nonpolar HgI (dashed line).

These simulations also contained information concerning the specific solvent motions that are responsible for the relaxation. The coupling to the solvent is strong as a result of the polarity of the system. However the solvent nuclear response is a few times faster than the vibrational period indicating that the HgI–ethanol system is close to the adiabatic regime. Somewhat surprisingly the excess vibrational energy appears to be dissipated mainly through the short range Lennard–Jones interactions with solvent oxygen atoms which are held close to the Hg by long-range Coulombic interactions [29]. The reason for this is discussed below.

In order to understand whether the forces causing the decay are short or long range, one needs to know the LJ and coulombic components of the force. Figure 5 shows the electrostatic contribution to the total friction spectrum. It is evident from this figure that short range LJ forces dominate the friction at the HgI oscillator frequency. Thus the existence of solute charges *per se* is not enough to bring about rapid relaxation unless the solvent has fluctuating charges at the appropriate frequency. The reason for the dominance of LJ forces in the vibrational relaxation of dipolar HgI can be explained from the structural information obtained from the simulation [29]. The strong coulombic interactions bring the oxygen atoms closer to the mercury to form a well defined structure which is enhanced by the H-bonding of solvent molecules themselves. As a result of their close proximity, the LJ forces between them are from the repulsive part of the LJ potential. Even though the LJ contribution to the interaction energy is much smaller than that of coulombic, the fluctuations in LJ forces are larger. Since the repulsive part of the potential is very steep, slight displacements in oxygen positions cause large fluctuations in force which dominate the friction spectrum in the region of interest.

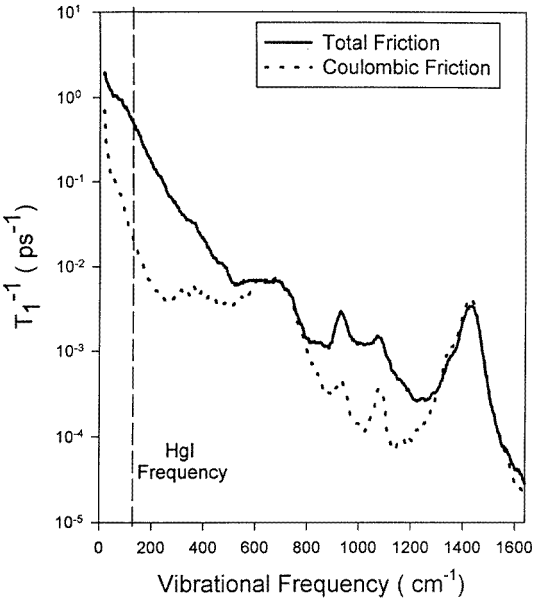


**Figure 5.** The contribution of Coulombic forces to the total friction spectrum of dipolar HgI, showing that the electrostatic contribution to vibrational energy relaxation in HgI is minimal.

The magnitude and direction of the short and long range forces on the HgI bond were also determined [29]. The electrostatic and LJ parts of the force on the vibrational

coordinate are in opposite directions, suggesting that LJ and electrostatic contributions to the intermolecular interaction cause opposing bond displacements. The coulombic force tends to extend the HgI bond while the LJ force tends to compress it. A possible reason for this difference is that the coulombic interactions tend to create isolated, solvated atoms. The simulations also give information about the mean square fluctuations of the different types of forces. Even though the mean value of the coulombic force is larger than its LJ counterpart, the mean square of the fluctuations of the LJ forces greatly exceeds that from the electrostatic part of the force. This is the manifestation of the fluctuation-dissipation theorem and is consistent with the spectrum shown in figure 5 and the discussion above, namely that it is the fluctuations and not the magnitude of the forces that are relevant.

*2.1.6. Orientational dynamics.* The time dependent anisotropies $r_e(t)$ of the transient absorption observed after excitation of $HgI_2$ at 270 nm and 320 nm are shown in figure 6 for representative probe wavelengths [30]. At the earliest times the anisotropy is seen to exhibit a sub-100 fs rise to a maximum from a small value. The rise occurs during the reactive period while the HgI and I fragments are separating [22]. This period is completed at approximately the time when the first maximum in the oscillatory signal occurs, which corresponds to HgI having reached its most extended configuration for the first time [22]. After the maximum in the anisotropy, the signal shape is not influenced by the reactive motion or the pulse shapes. The initial anisotropy indicates a $^1\Pi$ state contribution to the probe transitions from the $HgI_2$ reactive potential. The fast rise of the anisotropy corresponds to the reactive motion toward HgI in a $^2\Sigma$ state. The signal from the separating HgI and I fragments is freed from reactant excited state ($^1\Pi$ or $^1\Sigma$) character after about one quarter of the vibrational period of either the asymmetric stretch motion of $HgI_2$ (65 fs) or of free HgI (60 fs). The time of 65 fs measured here represents one reasonable assessment of the lifetime of the transition state for this reaction.

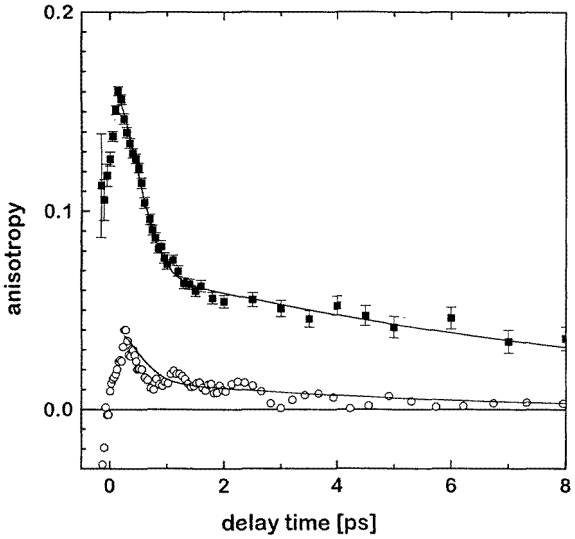


**Figure 6.** Anisotropies of the transient absorption observed after $HgI_2$ photolysis for 270 nm pump, 490 nm probe (■) and for 320 nm pump, 440 nm probe (○ ). The solid lines correspond to the best fit of the anisotropy decay after 150 fs to a sum of a gaussian and an exponential.

After the reactive portion is completed, the anisotropy clearly exhibits a biphasic decay dominated by a faster part with a half time of about 500 fs, followed by an exponential decay with a lifetime of 8–10 ps. This behaviour is reminiscent of that exhibited by other diatomic molecules in solution as seen from the Raman lineshape analysis [62, 66–70]. In general, at the earliest times, the fast decay resembles the decay of the free rotor rotational coherence at the temperature of the solvent bath. At intermediate times the decay deviates from that of the free rotor because the inertial motion soon becomes interrupted by solvent collisions and changes in the magnitude and direction of the rotational angular momentum take place [67]. The anisotropy calculated from the classical MD simulation is shown in figure 7, together with the simulated anisotropy of free rotor HgI. The average rotational period estimated from a Gaussian fit of the fast part of the MD-simulated anisotropy was $\sim 1.3$ ps compared to $\sim 1.5$ ps for the free rotor. The appearance of the slower component of the anisotropy decay is attributed to rotational diffusion dynamics [30].

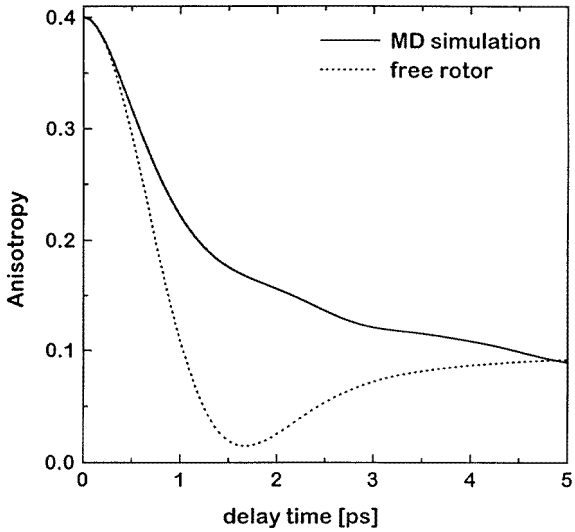


**Figure 7.** Anisotropy decay $2/5\langle P_2[\mu(0)\cdot\mu(t)]\rangle$ from an equilibrium MD simulation of HgI in ethanol. The dotted line shows the free rotor decay.

*2.1.7. Rotational energy decay.* The normalized angular momentum correlation function, $C_{JJ}(t)$, shown in figure 8 also provides additional information on the rotational dynamics. In the expression for $C_{JJ}(t)$,

$$C_{JJ}(t) = \frac{\langle \delta J(0)\cdot\delta J(t)\rangle}{\langle \delta J^2(0)\rangle} = \frac{\langle \delta\omega(0)\cdot\delta\omega(t)\rangle}{\langle \delta\omega^2(0)\rangle} \tag{9}$$

where $\delta J$ is the fluctuation of the angular momentum and $\delta\omega$ that of the angular velocity. It decays with a time constant of $\tau_J = 210$ fs. The strong torques imparted by the surrounding solvent molecules seem to be capable of reversing the sense of HgI rotation as shown by the fact that $C_{JJ}(t)$ becomes negative [60]. The damped oscillation can be interpreted as arising from the HgI molecules librating in the presence of the H-bonded solvent 'cage' and collisions may be correlated for a short time period [71, 72]. Also shown in figure 8 is the

rotational kinetic energy correlation function, $C_{EE}(t)$,

$$C_{EE}(t) = \frac{\langle \delta E(0)\, \delta E(t) \rangle}{\langle \delta E^2(0) \rangle} = \frac{\langle \delta J^2(0)\, \delta J^2(t) \rangle}{\langle \delta J^4(0) \rangle} \tag{10}$$

where $\delta E$ is the rotational energy fluctuation. $C_{EE}$ decays with a time constant ($\tau_E$) of $\sim 160$ fs. This time corresponds to the decay of excess rotational energy assuming a linear response. The timescale of $C_{EE}(t)$ predicts that if there were a rotationally hot product distribution, the solvent will relax the excess rotational energy very quickly.

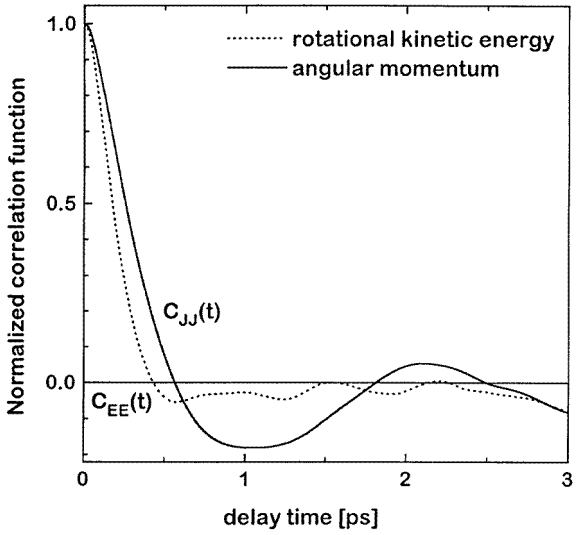


**Figure 8.** Normalized angular momentum correlation function $C_{JJ}(t)$ (solid line) and rotational kinetic energy correlation function $C_{EE}(t)$ (dotted line) calculated from MD.

The simulations incorporate equilibrium conditions while in the experiment the system is prepared impulsively and initially is known to have a nonequilibrium vibrational distribution [22]. It is of great interest to examine the nonequilibrium distribution of rotational excitations. If the HgI were born rotationally hot, it should lose rotational coherence faster than predicted from the bath temperature until the rotational energy relaxation is completed. The relevant information is contained in the rotational energy correlation function shown in figure 8 which decays in 160 fs. This result predicts that all the information about the initial distribution of rotational excitations is lost by 160 fs. The good agreement between the simulation and the experiment beyond 300 fs is certainly consistent with the system being rotationally equilibrated, although, in this case, the result is not surprising since the collinear dissociation of a nearly linear molecule into an atom and a diatom is unlikely to yield much rotational energy excess [1].

*2.1.8. Vibrating rotor dynamics.* It is evident from figure 9 that there is an oscillatory component on the early part of the anisotropy [30] that correlates with the motion of the HgI wavepacket. The instantaneous slope of the experimental anisotropy decay is systematically lowest when the molecule is most extended, corresponding to the maxima of the transient absorption oscillations [22, 23] and largest when the molecule is compressed. As the wavepacket moves from the repulsive to the attractive side of the potential, both the

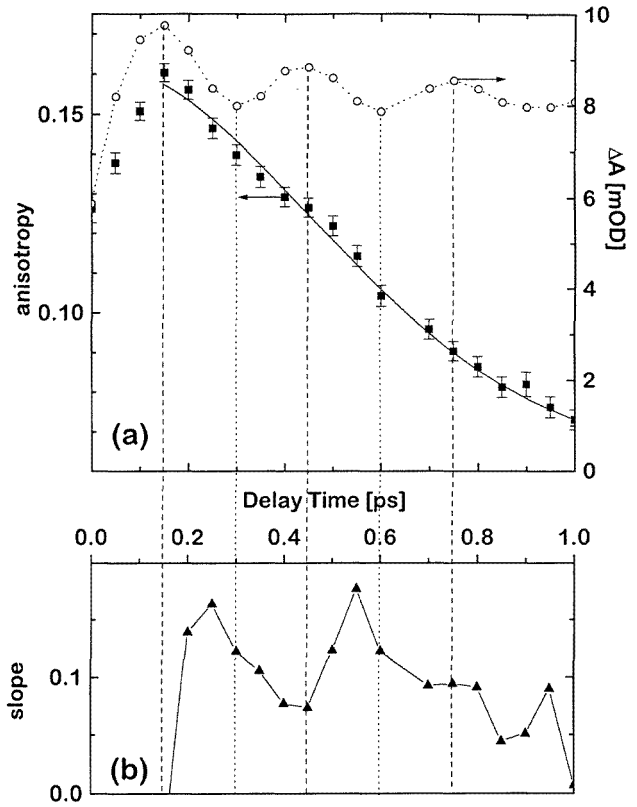


**Figure 9.** Oscillatory component in the HgI anisotropy decay. (a) Transient absorption (○, right axis), observed with magic angle polarization of pump and probe, and anisotropy (■, left axis). The solid line corresponds to the best fit of the anisotropy decay after 150 fs to a sum of a Gaussian and an exponential. (b) Slope of the anisotropy decay. The vertical lines indicate the delay times at which HgI is in its most extended (dashed lines) or most compressed (dotted lines) conformation.

moment of inertia and the hydrodynamic volume will increase and slow down the molecular reorientation. At the 490 nm probe wavelength the observed HgI molecules at the centre of the distribution are stretching from about 2.65 to 3.2 Å [22]. The Van der Waals length of HgI is 6.4 Å, so the wavepacket motion gives rise to an 8.5% peak-to-peak oscillation in the molecular volume. Since the rotational diffusion time is generally proportional to volume [73] this should result in an oscillation in the slope of the anisotropy decay of about the same magnitude. The inertial part of this effect is the time domain manifestation of a nonrigid rotor. We calculated the inertial rotational coherence decay of HgI treated as a free anharmonic nonrigid rotor and found oscillations in the slope of about the same as those that were estimated for diffusion. It appears both effects are occurring.

### *2.2. Photochemistry of $ClO^-$*

The experiments on the photodissociation of $ClO^-$ in water clearly monitor an internal excitation of $ClO^-$ more strongly coupled to the solvent coordinate than $HgI_2$. The transients

that could be probed are Cl atoms, solvated electrons and electronic and vibrational excited states of $ClO^-$ [32]. The probe wavelength dependence of the isotropic transients and a representative anisotropy, after photoexcitation, are shown in figure 10. The transients show an instrument-response-time-limited absorption, followed by a rapid decay, then a growth and decay. In the wavelength dependence of the longer time dynamics, the faster decay times ($\sim$ 1.3 ps) are observed for the lowest energy probes. The transient spectra at 3 ps and 10 ps corresponds to the spectrum of the Cl atom in water [74]. It is concluded that there is a photodissociation channel leading to $Cl + O^-$.

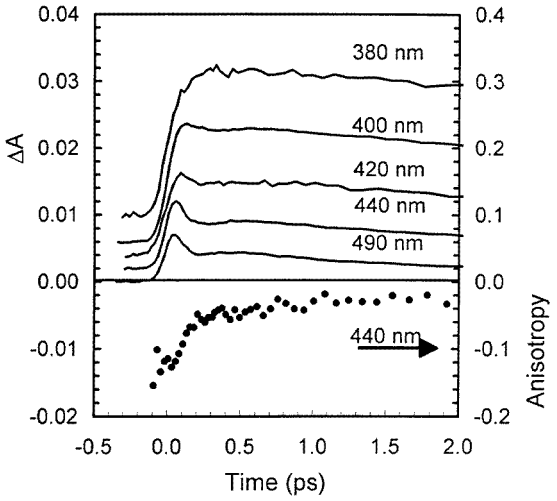


**Figure 10.** Probe wavelength dependent isotropic transient absorptions ($A$) and a representative anisotropy ($B$) of $ClO^-$ in water following 320 nm photolysis [32].

*2.2.1. Solvent response to charge shifting.* There are two time scales associated with charge shifting: that during which the solvent structure around the equilibrated ground state $ClO^-$ is destroyed and that during which the solvent molecules orient themselves around the newly formed $OCl^-$. The early time spike decays in 60 fs as the spectrum causing it shifts. This timescale and shift correspond to the solvent reorganization around the newly formed charge distribution of $OCl^-$ [32]. A similar fast response was seen in the solvation of a dye molecule in water and attributed to a rapid inertial motion [75]. The fast decay in the present case likely arises solely from destruction of the polarized solvent structure around the neutral O atom end of $OCl^-$. This is supported by the nonequilibrium MD simulations that considered the structural changes involved with the destruction and the formation of the first solvation shell following charge shifting of $ClO^-$ in water [32]. The calculated time dependence of the solute–solvent radial distribution function ($G(r)$) indicates that the solvent structure around $ClO^-$ in the ground state is destroyed much more rapidly than the new solvent structure around $OCl^-$ is created.

*2.2.2. Vibrational relaxation in $H_2O$ and $D_2O$.* The longer time dynamics with decay time constants between 1.3 and 7 ps have all the characteristics expected from relaxation of the vibrationally hot ground state of $ClO^-$ [32]. The faster decay times are observed for the lowest energy probe pulses, suggesting that they sample higher energy portions of the

ground electronic potential. The timescales for the decay of the transients due to hot ground state molecules are expected to depend on the probe wavelength, due to the vibrational quantum number dependence of the state-to-state rates [23]. The recovered growth time constant for all probe wavelengths is 290 fs. The vibrational relaxation time required for this interpretation is estimated to be a few ps.

As shown in figure 11, transients of $ClO^-$ in $D_2O$ show a similar ps timescale decay. In fact the data obtained with $H_2O$ and $D_2O$ are not significantly different over the whole time range investigated. The spectrum of the friction exerted by the solvent on the diatomic $ClO^-$ vibrational coordinate was calculated from classical equilibrium MD simulations. The relevant friction spectra of the $ClO^-$ bond in $H_2O$ and $D_2O$ are shown in figure 12. It is evident from the figure that in the range of 713 $cm^{-1}$ (the experimental vibrational frequency), the friction amplitudes happen to be similar in $H_2O$ and $D_2O$, even though the spectra are different.

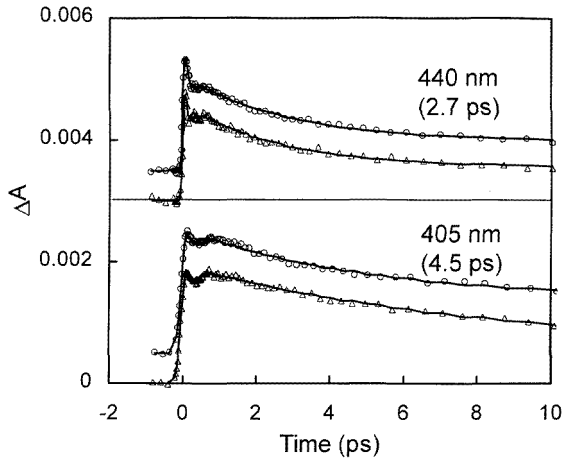


**Figure 11.** Isotropic transient absorption data in $D_2O$ (△) and $H_2O$ (○) and their fit at 440 nm and 405 nm. The longer time decay constants are also shown in parenthesis [32].

*2.2.3. Rotational dynamics.* The ionic $ClO^-$ in water has a strong solvent–solute interaction so it is unlikely that the $ClO^-$ molecule exhibits much inertial-like rotational motion. The anisotropy decay of an ensemble of $ClO^-$ in a collision-free gas at temperature 298 K is shown in figure 13 together with the experimental anisotropy data at 440 nm and an anisotropy decay obtained from equilibrium MD simulations. Since much of the observed anisotropy decay is faster than that of $ClO^-$ in gas phase at the same temperature, the early time decay cannot be caused by the inertial-like rotation. As expected, the MD simulation, also shown in figure 13, shows only a small inertial-like component. The remaining anisotropy in the sample decays within 6 ps which is the rotational diffusion of the $ClO^-$ molecule.

*2.2.4. Electron transfer.* The ground state $ClO^-$ is recovered in 290 fs in an ultrafast electron transfer process from $OCl^-$ [32]. This process involves the stretching of the $Cl–O^-$ bond in order to optimize the balance between the effective driving force ($\Delta G_{eff}$) for the electron transfer and the solvent reorganization energy ($\lambda_s$). In other words, the potential

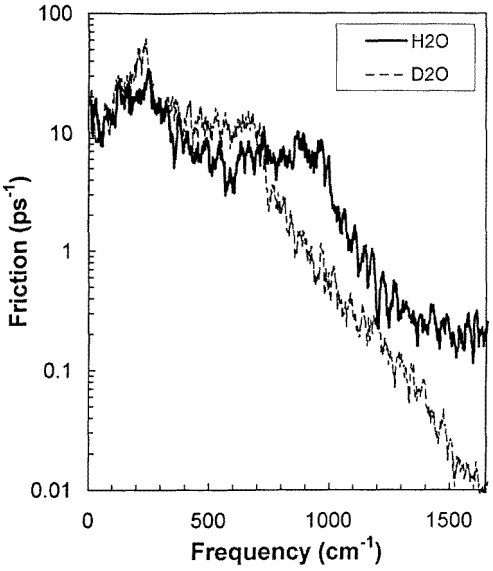


**Figure 12.** The spectrum of solvent friction for the vibrational coordinate of diatomic $ClO^-$. The solid line is for $H_2O$ and the dashed line for $D_2O$.

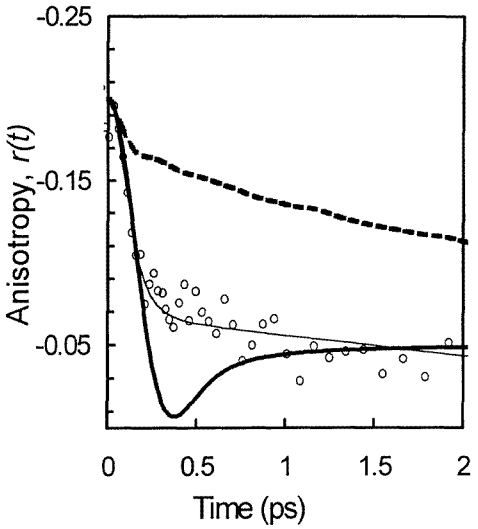


**Figure 13.** The rotational anisotropy of $ClO^-$ in a gas at room temperature (thick solid line) along with the experimental data (○ ) in $H_2O$ and fit to the data (thin solid line). The decay obtained from an MD simulation (dashed line) are also shown [32].

curves along the solvent coordinate of the ground and excited states cross with $\Delta G_{eff} = \lambda_s$ when the $ClO^-$ bond is optimally extended. This we believe is the reason why there is a large amount of vibrational energy found in the ground state after electron transfer.

## 3. Conclusions

Hopefully these examples have provided a flavour of current experiments on the chemical dynamics of small molecules in solutions. Further work will need to focus more on the reactive motions of the fragments and solvent, and on ways of deducing potential energy or free energy surfaces from experiments in which solvent is involved. Another avenue for future research must surely be nonadiabatic dynamics where the solvent and reactive motions occur in comparable time scales. Such a situation presents challenges to both theory and experiment: the theory will need to combine quantum chemistry and statistical mechanics and the experiments will require to expose the solvent participation directly.

## Acknowledgment

This research was supported by grants from NSF and NIH.

## References

[1] Levine R D and Bernstein R B 1987 *Molecular Reaction Dynamics and Chemical Reactivity* (New York: Oxford University Press)
[2] Polanyi J C and Zewail A H 1995 *Acc. Chem. Res.* **28** 119, and references therein
[3] Voth G A and Hochstrasser R M 1996 *J. Phys. Chem.* **100** 13 034. and references therein
[4] Grote R F and Hynes J T 1980 *J. Chem. Phys.* **73** 2715
[5] Hynes J T 1985 *Ann. Rev. Phys. Chem.* **36** 573
[6] Berne B J, Borkovec M and Straub J E 1988 *J. Phys. Chem.* **92** 3711
[7] Nitzan A 1988 *Adv. Chem. Phys.* **70** Part 2 489
[8] Onuchic J N and Wolynes P G 1988 *J. Phys. Chem.* **92** 6495
[9] Benjamin I, Barbara P F, Gertner B J and Hynes J T 1995 *J. Phys. Chem.* **99** 7557
[10] Whitnell R M, Wilson K R and Hynes J T 1992 *J. Chem. Phys.* **96** 5354
[11] Harris A L, Brown J K and Harris C B 1988 *Ann. Rev. Phys. Chem.* **39** 341
[12] Schwartz B J, King J C, Zhang J Z and Harris C B 1993 *Chem. Phys. Lett.* **203** 503
[13] Banin U, Waldman A and Ruhman S J 1992 *J. Chem. Phys.* **96** 2416
[14] Banin U and Ruhman S 1993 *J. Chem. Phys.* **98** 4391
[15] Banin U, Kosloff R and Ruhman S 1994 *Chem. Phys.* **183** 289
[16] Alfano J C, Kimura Y, Wallhout P K and Barbara P F 1993 *Chem. Phys.* **175** 147
[17] Kliner D A V, Alfano J C and Barbara P F 1993 *J. Chem. Phys.* **98** 5375
[18] Walhout P K, Alfano J C, Thakur K A M and Barbara P F 1995 *J. Phys. Chem.* **99** 7568
[19] Walhout P K, Silva C and Barbara P F 1996 *J. Phys. Chem.* **100** 5188
[20] Dunn R C, Flanders B N and Simon J D 1995 *J. Phys. Chem.* **99** 7360
[21] Owrutsky J C, Raftery D and Hochstrasser R M 1994 *Ann. Rev. Phys. Chem.* **45** 519
[22] Pugliano N, Szarka A Z and Hochstrasser R M 1996 *J. Chem. Phys.* **104** 5062
[23] Pugliano N, Szarka A Z, Gnanakaran S, Treichel M and Hochstrasser R M 1995 *J. Chem. Phys.* **103** 6498
[24] Pugliano N, Szarka A Z, Palit D K and Hochstrasser R M 1993 *J. Chem. Phys.* **99** 7273
[25] Pugliano N, Gnanakaran S and Hochstrasser R M 1996 *J. Photochem. Photobiol.* in press
[26] Dantus M, Bowman R M, Gruebele M and Zewail A H 1989 *J. Chem. Phys.* **91** 7437
[27] Bowman R M, Dantus M and Zewail A H 1989 *Chem. Phys. Lett.* **156** 131
[28] Gruebele M, Roberts G and Zewail A H 1990 *Phil. Trans. R. Soc.* A **332** 223
[29] Gnanakaran S and Hochstrasser R M 1996 *J. Chem. Phys.* **105** 3486
[30] Volk M, Gnanakaran S, Gooding E, Kholodenko Y, Pugliano N and Hochstrasser R M 1996 *J. Phys. Chem.* in press
[31] Lim M, Pugliano N, Gnanakaran S and Hochstrasser R M 1996 *Ultrafast Phenomena* vol X, ed W Zinth *et al* (Berlin: Springer) in press
[32] Lim M, Gnanakaran S and Hochstrasser R M 1996 *J. Chem. Phys.* submitted
[33] Peterson K A and Woods R C 1990 *J. Chem. Phys.* **92** 7412
[34] Maroncelli M, MacInnis J and Fleming G R 1989 *Science* **243** 1674
[35] Wynne K and Hochstrasser R M 1993 *Chem. Phys.* **171** 179

[36] Hochstrasser R M, Pereira M A, Share P E, Sarisky M J, Kim Y R, Repinec S T and Sension R J 1991 *Proc. Indian Acad. Sci.* **103** 351
[37] Sension R J, Repinec S T, Szarka A Z and Hochstrasser R M 1993 *J. Chem. Phys.* **98** 6291
[38] Cross A J, Waldeck D H and Fleming G R 1983 *J. Chem. Phys.* **78** 6455
[39] Garraway B M and Suominen K 1995 *Rep. Prog. Phys.* **58** 365
[40] Kosloff D and Kosloff R 1983 *J. Comp. Chem.* **52** 35
[41] Cohen-Tannoudji C, Dupont-Roc J and Grymberg G 1993 *Photon-Atom Interactions* (New York: Wiley)
[42] Redfield A G 1965 *Adv. Mag. Res.* **1** 1
[43] Chandrasekhar S 1943 *Rev. Mod. Phys.* **15** 1
[44] Note that equation (19) of reference [3] and equation (19) of reference [22] should read as

$$\frac{\mathrm{d}}{\mathrm{d}t}\langle b\rangle(t) = -\left(\mathrm{i}\omega_0 + \frac{1}{2T_1} + \frac{1}{T_2'}\right)\langle b\rangle(t)$$

[45] Chandler D 1978 *Ann. Rev. Phys. Chem.* **29** 441
[46] Berne B J 1970 *Adv. Chem. Phys.* **17** 63
[47] Bergsma J P, Reimers J R, Wilson K R and Hynes J T 1986 *J. Chem. Phys.* **85** 5625
[48] Bergsma J P, Gertner B J, Wilson K R and Hynes J T 1987 *J. Chem. Phys.* **86** 1356
[49] Gertner B J, Wilson K R and Hynes J T 1989 *J. Chem. Phys.* **90** 3537
[50] Whitnell R M, Wilson K R and Hynes J T 1990 *J. Phys. Chem.* **94** 8625
[51] Landau L and Teller E 1936 *Z. Sowj.* **10** 34
[52] Oxtoby D W 1981 *Adv. Chem. Phys.* **47** 487
[53] Metiu H, Oxtoby D W and Freed K F 1977 *Phys. Rev.* A **15** 361
[54] Zwanzig R W 1961 *J. Chem. Phys.* **34** 1931
[55] Zwanzig R W 1959 *Phys. Fluids* **2** 12
[56] Grote R F and Hynes J T 1982 *J. Chem. Phys.* **77** 3736
[57] Bader J S and Berne B J 1994 *J. Chem. Phys.* **100** 8359
[58] Benjamin I and Whitnell R M 1993 *Chem. Phys. Lett.* **204** 45
[59] Ferrario M, Klein M L and McDonald I R 1993 *Chem. Phys. Lett.* **213** 537
[60] Allen M P and Tildesley D J 1987 *Computer Simulation of Liquids* (Oxford: Clarendon)
[61] Steele W A and Streett W B 1980 *Mol. Phys.* **39** 279
[62] Steele W A 1991 *J. Mol. Liquids* **48** 321
[63] Kabadi V N and Steele W A 1985 *J. Phys. Chem.* **89** 1467
[64] Frenkel D and McTague J P 1980 *J. Chem. Phys.* **72** 2801
[65] Barojas J, Levesque D and Quentrec B 1973 *Phys. Rev.* A **7** 1092
[66] Temkin S I and Steele W A 1993 *Chem. Phys. Lett.* **215** 285
[67] Gordon R G 1966 *J. Chem. Phys.* **44** 1830
[68] Gordon R G 1965 *Adv. Mag. Res.* **3** 1
[69] Gordon R G 1965 *J. Chem. Phys.* **42** 3658
[70] Gordon R G 1965 *J. Chem. Phys.* **43** 1307
[71] Lindenberg K and Cukier R I 1975 *J. Chem. Phys.* **62** 3271
[72] Lynden-Bell R M and Steele W A 1984 *J. Phys. Chem.* **88** 6514
[73] Berne B J and Pecora R 1976 *Dynamic Light Scattering* (New York: Wiley)
[74] Treinin A and Hayon E 1975 *J. Am. Chem. Soc.* **97** 1716
[75] Jimenez R and Fleming G R 1994 *Nature* **369** 471